Am J Cancer Res 2026;16(6):2258-2277
www.ajcr.us /ISSN:2156-6976/ajcr0173472

Original Article

NDUFA12 is associated with poor prognosis and promotes malignant phenotypes and mitochondrial metabolic alterations in hepatocellular carcinoma

Xiaomeng Liu[1*], Tianyi Liu[1*], Zihan Sun[2*], Nuersimanguli Maimaitiming[1*], Huayuan Liu[1], Deyang Kong[3], Yuan Wang[2], Jianqiang Cai[1], Hong Zhao[1]

[1]Department of Hepatobiliary Surgery, National Cancer Center/National Clinical Research Center for Cancer/Cancer Hospital, Chinese Academy of Medical Sciences and Peking Union Medical College, Beijing 100021, China; [2]Department of Pathology, National Cancer Center/National Clinical Research Center for Cancer/Cancer Hospital, Chinese Academy of Medical Sciences and Peking Union Medical College, Beijing 100021, China; [3]Department of Colorectal Surgery, National Cancer Center/National Clinical Research Center for Cancer/Cancer Hospital, Chinese Academy of Medical Sciences and Peking Union Medical College, Beijing 100021, China. [*]Equal contributors.

Received April 21, 2026; Accepted May 28, 2026; Epub June 15, 2026; Published June 30, 2026

Abstract: Hepatocellular carcinoma (HCC) is a leading cause of cancer-related death worldwide, yet effective treatment options remain limited. NDUFA12, a subunit of mitochondrial complex I, plays a crucial role in oxidative phosphorylation and cellular energy metabolism; however, its expression pattern, clinical significance, and biological role in HCC remain unclear. In this study, the expression profile and clinical relevance of NDUFA12 were analyzed using The Cancer Genome Atlas (TCGA) data. Genomic and functional features, including differentially expressed genes (DEGs), tumor mutation burden (TMB), functional enrichment, and immune infiltration, were assessed. An institutional cohort of 25 patients with advanced HCC receiving targeted-immunotherapy at our hospital was enrolled, and baseline tumor samples were subjected to RNA sequencing for validation. MHCC-97H and PLC/PRF/5 cells were transfected with small interfering RNAs (siRNAs) targeting NDUFA12. Functional assays, including CCK-8, EdU, wound healing, Transwell assays, Seahorse XF mitochondrial stress tests, Seahorse XF glycolysis stress tests, ATP production, lactate accumulation, mitochondrial membrane potential, and reactive oxygen species (ROS) detection, were performed to evaluate malignant phenotypes and metabolic alterations. NDUFA12 expression was markedly elevated in HCC and was associated with advanced tumor stage, increased TMB, and poorer overall survival and progression-free survival. DEG analysis suggested enrichment in cell cycle-, mitochondrial-, and metabolism-related pathways. Low NDUFA12 expression was associated with distinct immune infiltration patterns according to the CIBERSORT algorithm, and RNA-sequencing data of our cohort further confirmed longer overall survival in patients with low NDUFA12 expression. Functionally, NDUFA12 knockdown reduced cell proliferation, invasion and migration in HCC cells. Metabolic assays showed that NDUFA12 knockdown decreased oxygen consumption rate, ATP production, mitochondrial membrane potential, and intracellular ROS levels, while increasing extracellular acidification rate and lactate production, suggesting impaired mitochondrial respiration and compensatory glycolytic activation. Collectively, these findings suggest that NDUFA12 is associated with poor prognosis, malignant cellular phenotypes, and mitochondrial metabolic alterations in HCC. NDUFA12 may serve as a prognostic biomarker and a candidate target for further functional and translational investigation in HCC.

Keywords: NDUFA12, hepatocellular carcinoma, mitochondrial dysfunction, immunotherapy, oxidative phosphorylation, tumor microenvironment

Introduction

Hepatocellular carcinoma (HCC) ranks among the most frequent cancers of the digestive tract and persists as a major driver of cancer mortality around the world. According to GLOBOCAN 2022 statistics, HCC ranks the sixth in incidence among all tumor types (865,269; 4.3% of all sites) and third in mortality (757,948; 7.8% of all sites) [1]. In China, it is estimated that the

https://doi.org/10.62347/CMZB1297

incidence of HCC ranked the fourth with 368,000 new cases in 2022. The mortality of HCC ranked the second with 317,000 estimated deaths. Although a decrease in the incidence of HCC was observed, a high mortality continues to be observed [2]. Besides, due to the asymptomatic characteristic of HCC, the disease is usually in its advanced stage by the time it is detected, thus making surgical intervention impossible. Since 2020, the IMbrave150 had made significant progress in treating unresectable HCC patients [3]. Simultaneously, a randomized, phase 2-3 study ORIENT-32 was conducted in China to assess the efficacy of immune-targeted combination therapy compared to sorafenib in unresectable hepatocellular carcinoma. Results suggest that sintilimab plus the bevacizumab biosimilar IBI305 could improve the prognosis of patients with hepatitis B virus (HBV)-related unresectable HCC, further laying the groundwork for combination therapy to become the first-line treatment [4]. Nevertheless, the treatment prospects for patients with HCC is still gloomy, making the hunt for novel molecular targets all the more imperative.

Tumor vasculature and immune cells engage in bidirectional crosstalk that critically influences anti-tumor immunity, making immune-targeted combination therapy particularly imperative in HCC. On the one hand, dysfunctional tumor vessels impair $CD8^+$ T cell infiltration into the tumor microenvironment (TME), reducing their effector activity and promoting cell death. Additionally, vascular endothelial growth factor (VEGF) not only disrupts dendritic cell maturation and T cell priming but also promotes $CD8^+$ T cell exhaustion [5]. Conversely, both innate and adaptive immune cells actively participate in generating abnormal tumor vasculature. Pro-angiogenic factors secreted by M2 macrophages, Th2 cells, and regulatory T (Treg) cells drive uncontrolled, immature vessel formation, while interferon-gamma (IFN-γ) from $CD8^+$ and $CD4^+$ Th1 cells suppresses angiogenesis and facilitates vascular normalization [6]. These findings have prompted preclinical evidence that concurrent targeting of both tumor vasculature and immune components is a viable approach to correct these disrupted interactions and improve immunotherapy outcomes.

The liver is responsible for a range of physiological processes, including metabolic processes, detoxication, glycogen storage, blood coagulation factor production, and immune functions [7], which requires substantial energy supply, positioning mitochondria at the core of cellular energy metabolism. Increasing evidence indicates that mitochondrial dysfunction and metabolic reprogramming are two important contributors to HCC progression [8]. Alterations in oxidative phosphorylation, redox homeostasis, mitophagy regulation, and mitochondrial dynamics have been implicated during this progression [9]. NDUFA12, a subunit of mitochondrial complex I (CI) [10], participates in electron transport and ATP generation through oxidative phosphorylation. It has been previously reported that NDUFA12 is essential for the proper assembly of CI and mitochondrial function [11], while loss of NDUFA12 [12] or NDUFA12 mutations [13] are closely related to mitochondrial diseases such as Leigh syndrome, a progressive, neurodegenerative disorder of the central nervous system [14]. Recently, emerging evidence has suggested a potential link between NDUFA12 and cancer biology. Se et al. revealed that in HepG2 cells, NDUFA12 could be repressed by directly binding to Ertredin (a growth inhibitor selective for EGFRvIII-mutant cancer cells), therefore suppressing cancer cell survival [15]. Later they made a step forward and compared the antitumor activity of Ertredin with 7MeERT, a methylated analogue of Ertredin. Results demonstrated that 7MeERT showed an improved anti-proliferative effect than Ertredin, similarly via a direct binding to NDUFA12 and inhibition of oxidative phosphorylation [16]. Nevertheless, the expression profiles, clinical significance, and biological role of NDUFA12 in HCC await further elucidation.

Therefore, we systematically explored the expression profile and clinical role of NDUFA12 in HCC. We further investigated its connection with clinicopathological characteristics and patient prognosis. Functional assays were conducted to evaluate the role of NDUFA12 in cancer cell proliferation, migration, invasion, and metabolic phenotypes of HCC cells. Our findings aim to yield novel insights into the potential impact of NDUFA12 on HCC and its value as a candidate treatment target.

Materials and methods

Bioinformatics analysis

The Cancer Genome Atlas (TCGA) public database was mined for bioinformatics analysis,

including differentially expressed gene (DEG), immune infiltration of the TME, and tumor mutation burden (TMB) analyses. The GEPIA3 tool (https://gepia3.bioinfoliu.com/) was preliminarily utilized to explore NDUFA12 expression across various cancers, as well as to conduct overall survival (OS) and progression-free survival (PFS) analyses in liver hepatocellular carcinoma (LIHC) patients with different NDUFA12 expression levels [17]. The expression profiles, along with the clinical data of 363 HCC cases from the TCGA database were downloaded via the GDC portal (https://portal.gdc.cancer.gov/). The expression datasets were normalized and converted using log2 transformation for subsequent analysis. Thereafter, NDUFA12 expression was compared between paired normal and tumor samples. Patients were stratified based on the median expression level, and clinicopathological characters, including age, gender, grade, stage and TNM, were analyzed between different groups of patients. Pearson correlation test was applied to screen for genes strongly correlated with NDUFA12, defined by |Pearson R| > 0.6 and P < 0.001. Perl (version 5.30.1) and R (version 4.2.2) were used for data processing, analysis, and plotting.

DEG analysis and functional enrichment

DEG analysis were conducted among patients between high- and low-expression groups using the "limma" package [18]. Genes fulfilling the following criteria were classified as DEGs: |log2 fold change (FC)| > 1 and false discovery rate (FDR) < 0.05. The top 25 DEGs were visualized by a heatmap using the "pheatmap" package. Gene Ontology (GO) enrichment analysis was conducted across the biological process (BP), cellular component (CC), and molecular function (MF) categories, as well as Kyoto Encyclopedia of Genes and Genomes (KEGG) pathway enrichment analysis. The "clusterProfiler" package was utilized for conducting the aforementioned analysis [19], and the "enrichplot", "ggplot2", "ComplexHeatmap" [20], and "circlize" [21] packages were deployed for visualization. Both *P* and adjusted *P* (*P*.adj) values < 0.05 were considered statistically significant.

Immune infiltration and TMB analyses

For immune infiltration analysis, the "estimate" package was used to calculate the stromal (stromal cell infiltration in tumor samples), immune (immune cell infiltration in tumor samples) and estimate (tumor purity) scores [22]. The CIBERSORT algorithm served to quantify the infiltration levels of 22 immune cell subtypes [23], whose correlations with NDUFA12 expression was assessed by the Spearman correlation test and Wilcoxon test. Immunogenomic profiles of hepatocellular carcinoma patients were retrieved from The Cancer Immunome Atlas (TCIA) (https://tcia.at/home). Patients with different NDUFA12 expression levels were compared for differences in TME [24]. Correlations of the expression of NDUFA12 with immune checkpoints were determined by a Pearson correlation test, with $P < 0.001$ deemed to be significant. TMB, defined as the total number of somatic mutations per million bases, was analyzed with the "maftools" package [25]. The correlation between TMB and NDUFA12 expression was analyzed, along with the comparison of TMB between different expression groups.

Patients

Among advanced HCC patients admitted to Cancer Hospital, Chinese Academy of Medical Sciences and Peking Union Medical College from May 2021 to November 2021, twenty-five patients receiving PD-(L)1 inhibitor combined with either bevacizumab or a tyrosine kinase inhibitor (TKI) were retrospectively reviewed, and patients with tumor specimens available were enrolled in our study. All patients were diagnosed as HCC histologically. The clinical characteristics of each patient, including gender, age, Child-Pugh, BCLC, infection status, extrahepatic disease, ECOG, AFP and treatment lines were collected. The best overall responses (BORs) of all patients were evaluated and patients were followed up according to the mRECIST standard. This work was conducted in accordance with the Declaration of Helsinki. The protocol was approved by the Ethics Committee of the Cancer Hospital, Chinese Academy of Medical Sciences (Approval No. 21/197-2868). The signed informed consent forms were provided by all patients.

RNA-sequencing assay

RNA was isolated from formalin-fixed paraffin-embedded (FFPE) samples using the Qiagen

AllPrep DNA/RNA FFPE Kit (Hilden, Germany). Subsequently, the Qubit RNA HS assay (Thermo Fisher Scientific, Waltham, MA, USA) and the LabChip GXII touch 24 system (Perkin Elmer, Waltham, MA, USA) were employed to evaluate quantity and quality of extracted RNA, respectively. The fragmented RNA underwent a series of specialized procedures, including the processes of synthesizing strand-specific cDNA, adding dA tails, ligating unique molecular identifier (UMI) adaptors, amplifying via polymerase chain reaction (PCR), and hybridizing with capture probes. Subsequently, the prepared NGS libraries were sequenced on an Illumina NovaSeq 6000 system (San Diego, CA, USA). A minimum threshold of more than 25 million reads per sample was established to ensure data quality. Following sequencing, data refinement steps were implemented, encompassing the deduplication of sequences, the stripping of UMI sequences from headers, and the removal of both adaptors and reads of low quality. The resulting clean reads were mapped to the human reference genome 19 via STAR (version 2.7.3a). Subsequently, based on the UMI sequences and read alignment positions, consensus reads were generated, followed by a second alignment to the human reference genome 19, performed with STAR2 (version 2.7.3a). The expression value of genes was normalized by log2 transformation.

Cell culture and transfection

The human HCC cell line PLC/PRF/5 (Cat. No. 1101HUM-PUMC000674) was sourced from Chinese Academy of Medical Sciences. The MHCC-97H cell line was obtained from Prof. Song at Chinese Academy of Medical Sciences. Cells were maintained at 37°C in a humidified atmosphere containing 5% CO_2, using DMEM (BasalMedia Technologies, Shanghai, China, Cat. No. L610KJ) with the addition of 10% fetal bovine serum (FBS; Gibco, USA, Cat. No. A5256701) and 1% penicillin-streptomycin (Gibco, USA, Cat. No. 15140-122). Cells were digested with 0.25% trypsin (BasalMedia Technologies, Shanghai, China, Cat. No. S320KJ) and passaged at a 1:3 ratio upon reaching 80-90% confluence. For NDUFA12 knockdown, commercially synthesized small interfering RNAs (siRNAs) targeting human NDUFA12, along with a negative control siRNA were obtained from Genechem (Shanghai Genechem Co., Ltd., China), and the sequences were provided in Table S1. These siRNAs were separately transfected into MHCC-97H and PLC/PRF/5 cells using Lipofectamine 3000 transfection reagent (Invitrogen, USA, Cat. No. L3000008) in line with the manufacturer's instructions.

RNA extraction and quantitative real-time PCR

Extraction of total RNA was performed employing the AG RNAex Pro Reagent (ACCURATE BIOTECHNOLOGY (HUNAN) Co., Ltd., Changsha, China, Cat. No. AG21101) conforming to the manufacturer's instructions. The HiScript III SuperMix Perfect for qPCR Kit (Vazyme Biotech Co., Ltd., China, Cat. No. R333-01) was used for reverse transcription. Quantitative PCR was carried out with Hieff qPCR SYBR Green Master Mix (Yeasen Biotechnology (Shanghai) Co., Ltd., China, Cat. No. 11202ES03) on a Real-Time PCR System. Each 20 μL quantitative PCR (qPCR) reaction contained 10 μL SYBR Premix Ex Taq II (2×), 0.8 μL forward primer (10 μM), 0.8 μL reverse primer (10 μM), 0.4 μL ROX Reference Dye II (50×), 2 μL cDNA template, and 6 μL sterile distilled water. Each sample was analyzed in triplicate. The PCR cycling conditions were as follows: initial denaturation at 95°C for 2 min, followed by 40 cycles of denaturation at 95°C for 5 s and annealing/extension at 60°C for 34 s. A melting curve analysis was then performed at 95°C for 15 s, 60°C for 1 min, and 95°C for 15 s to confirm amplification specificity. The $2^{-\Delta\Delta Ct}$ method was applied to calculate the relative expression of target genes after normalization to human β-actin. The primer sequences used were provided in Table S1.

Protein extraction and western blot

Cells were lysed in 200 μL of 1× SDS lysis buffer for protein extraction. The lysates were supplemented with 1 μL of 100× Protease Inhibitor Cocktail (TargetMol, Shanghai, China, Cat. No. C0001), and denatured by boiling at 100°C for 10 min. The mixture underwent centrifugation at 12,000 rpm for 10 min. The supernatant was then aspirated, and protein concentration was assayed using a BCA Protein Assay Kit (Epizyme, Shanghai, China, Cat. No. ZJ101) by a standard curve. A 10% sodium dodecyl sulfate polyacrylamide gel (SDS-PAGE; Epizyme, Shanghai, China, Cat. No. PG212) served for protein electrophoresis. Following transfer onto a PVDF

membrane (Millipore, Cat. No. ISEQ00010), the membrane was blocked with 5% non-fat milk for 2 h at room temperature. Subsequently, it was incubated overnight at 4°C with primary antibodies targeting NDUFA12 (Proteintech, Wuhan, China, Cat. No. 15793-1-AP; 1:800) and Tubulin (Proteintech, Wuhan, China, Cat. No. 66031-1-Ig; 1:2000). After washing, the membrane was incubated with horseradish peroxidase-conjugated goat anti-mice IgG (ZSGB-Bio, Beijing, China, 1:10000 dilution; Cat. ZB-2305) or anti-rabbit IgG (ZSGB-Bio, Beijing, China, 1:10000 dilution; Cat. ZB-2301) for 2 h at room temperature. An enhanced chemiluminescence detection reagent (Proteintech, Wuhan, China, Cat. No. PK10003) was used to visualize the immunoreactive bands, and signals were captured with a Tanon 5200 Chemiluminescence Imaging System (Tanon, Shanghai, China).

Cell proliferation assay

Using the CCK-8 assay, we evaluated the viability of MHCC-97H and PLC/PRF/5 cells on days 1, 2, 3, and 4 after planting them in 96-well plates at a density of 2,000 cells per well. Briefly, the medium in each well was replaced with 100 μL of a mixture containing CCK-8 reagent (Epizyme, Shanghai, China, Cat. No. CX001) and fresh DMEM medium (1:9 ratio). After incubating at 37°C for 1 h in a 5% CO_2 humidified incubator, absorbance readings at 450 nm and the reference wavelength of 630 nm were acquired via a microplate reader. For EdU assay, MHCC-97H and PLC/PRF/5 cells were seeded into 12-well plates at a density of 1×10^5 cells per well. After cell adhesion, the cell proliferation EdU assay was performed in line with the instructions (BeyoClic EdU-594 Cell Proliferation Assay Kit Cat. C0078S). The EdU-positive cell rate was calculated to evaluate cell proliferation.

Wound healing and transwell

Cell migration was evaluated using a wound healing assay. Transfected cells were cultivated in plates until confluency reached approximately 90%. A linear wound was introduced into the monolayer using a sterile 20-μL pipette tip. After washing gently with PBS (Servicebio, Cat. No. G4202) to remove floating cells, the plates were replenished with serum-free DMEM and then transferred back to the incubator. The wound area was observed and photographed under a microscope at 0 and 24 h. Scratch width was measured at multiple predefined points using the ImageJ software. The percentage of wound closure was then calculated to quantify the migration rate. For Transwell assays, NDUFA12-NC and siNDUFA12 HCC cells (1.5×10^5/well) were resuspended in serum-free DMEM and loaded into the upper Transwell chambers (8 μm pore size; Corning, USA, Cat. No. 3422), which were either precoated or uncoated with Matrigel for invasion or migration assays, respectively. After adding 20% FBS/DMEM (chemoattractant) to the lower chamber and allowing 24 h of incubation, cells on the upper-side were swabbed away, and the invading cells on the lower-side were fixed with 4% paraformaldehyde (Servicebio, Wuhan, China, Cat. No. G1101) for 20 min and stained with 0.2% crystal violet (Beyotime Biotechnology, Shanghai, China, Cat. No. C0121) for 10 min. Following washes with PBS for three times, the stained cells were imaged under a microscope and counted using ImageJ software.

Seahorse XF analyzer assay

To evaluate mitochondrial function after NDUFA12 knockdown, a Seahorse XF Cell Mito Stress Test was performed. Briefly, cells were seeded into an XF 24-well cell culture microplate and allowed to adhere overnight in a 37°C incubator with 5% CO_2. On the day of the assay, the growth medium was replaced with prewarmed Seahorse XF assay medium. Oxygen consumption rate (OCR) and extracellular acidification rate (ECAR) were measured in real time using an XF24 Extracellular Flux Analyzer (Agilent Technologies, CA, USA). The Mitochondrial Stress Test profile was generated by injecting the following compounds sequentially: 1.25 μM oligomycin (ATP synthase inhibitor), 2 μM carbonyl cyanide-p-trifluoromethoxy phenylhydrazone (FCCP; uncoupler), and a mixture of 1 μM rotenone and 1 μM antimycin A (complex I and III inhibitors). OCR values were normalized to the cell counts in each well. For the Glycolysis Stress Test, cells were treated with 10 mM glucose, 1.5 μM oligomycin, and 50 mM 2-deoxy-glucose (2-DG) in sequence for measurement of ECAR.

ATP production assay

Cellular ATP levels were determined using an ATP assay kit according to the manufacturer's

protocol (Beyotime Biotechnology, Shanghai, China, Cat. No. S0026). Briefly, cells were lysed on ice with ATP detection lysis buffer and centrifuged at 12000×g for 5 min at 4°C. The supernatants were collected for ATP measurement. ATP standards were prepared using ATP detection lysis buffer, and the ATP detection working solution was prepared. A total of 100 μL ATP detection working solution was added to each well and incubated at room temperature for 5 min to reduce background luminescence. Then, 20 μL sample or standard was added and rapidly mixed, and luminescence was measured using a luminometer. ATP concentrations were calculated based on the standard curve and normalized to total protein concentration determined by BCA assay.

Lactate accumulation assay

L-lactate levels were measured using a commercial lactate assay kit according to the manufacturer's instructions (Beyotime Biotechnology, Shanghai, China, Cat. No. S0208S). Briefly, cells were lysed on ice with lysis buffer 10 min, followed by centrifugation at 12000×g for 5 min at 4°C. The supernatants were collected for subsequent measurement. L-lactate standard solution underwent a gradient dilution for the preparation of the standard curve. For each sample or standard, 50 μL was added to a 96-well plate. Then, 50 μL freshly prepared WST-8 working solution was added to each well and mixed thoroughly. The plate was incubated at 37°C for 30 min in the dark, and the absorbance was measured at 450 nm using a microplate reader. The lactate concentration of each sample was calculated based on the standard curve after subtracting the blank background. Lactate levels were normalized to total protein concentration determined by BCA assay.

Mitochondrial membrane potential assay

Mitochondrial membrane potential was evaluated using a TMRE mitochondrial membrane potential assay kit (Beyotime Biotechnology, Shanghai, China, Cat. No. C2001S). Briefly, cells were incubated with freshly prepared TMRE staining working solution at 37°C for 30 min in the dark. After staining, cells were washed twice with pre-warmed culture medium and observed under a fluorescence microscope using the red fluorescence channel. Images were acquired under identical exposure settings, and relative fluorescence intensity was quantified using the ImageJ software after background subtraction.

Reactive oxygen species (ROS) detection

Intracellular ROS levels were measured using a DCFH-DA ROS assay kit (Beyotime Biotechnology, Shanghai, China, Cat. No. S0034S). Briefly, cells were incubated with 10 μM DCFH-DA working solution at 37°C for 20 min in the dark. After staining, cells were washed three times with PBS to remove excess probe. Fluorescence images were acquired using a fluorescence microscope with the green fluorescence channel. Images were captured under identical exposure settings, and relative fluorescence intensity was quantified using the ImageJ software after background subtraction.

Statistical analysis

Perl (version 5.32.1) and R (version 4.2.2) were used for bioinformatics analyses and visualization, and all R packages used were indicated in the earlier sections. Data are presented as the mean ± standard deviation (SD) unless otherwise indicated. All in vitro experiments were independently repeated at least three times. Differences between two groups were analyzed using Student's t-test or Wilcoxon rank-sum test, as appropriate. For comparisons among multiple groups, one-way ANOVA followed by post hoc multiple comparisons was used. Cell proliferation curves were analyzed using two-way repeated measures ANOVA. Survival differences were evaluated using the Kaplan-Meier method with the log-rank test. Correlation analyses were performed using Pearson or Spearman correlation tests. A two-sided P value < 0.05 was considered statistically significant unless otherwise indicated.

Results

NDUFA12 is aberrantly expressed and associated with prognosis in pan-cancer and HCC

Regarding the pan-cancer expression pattern of NDUFA12, expression levels were comparable between tumor and normal samples in diffuse large B-cell lymphoma (DLBC), pheochromocytoma and paraganglioma (PCPG), etc. NDUFA12 was upregulated in the left types of cancers, including LIHC, except acute myeloid leukemia (LAML) and sarcoma (SARC) (**Figure 1A**). The comparison in paired normal and LIHC

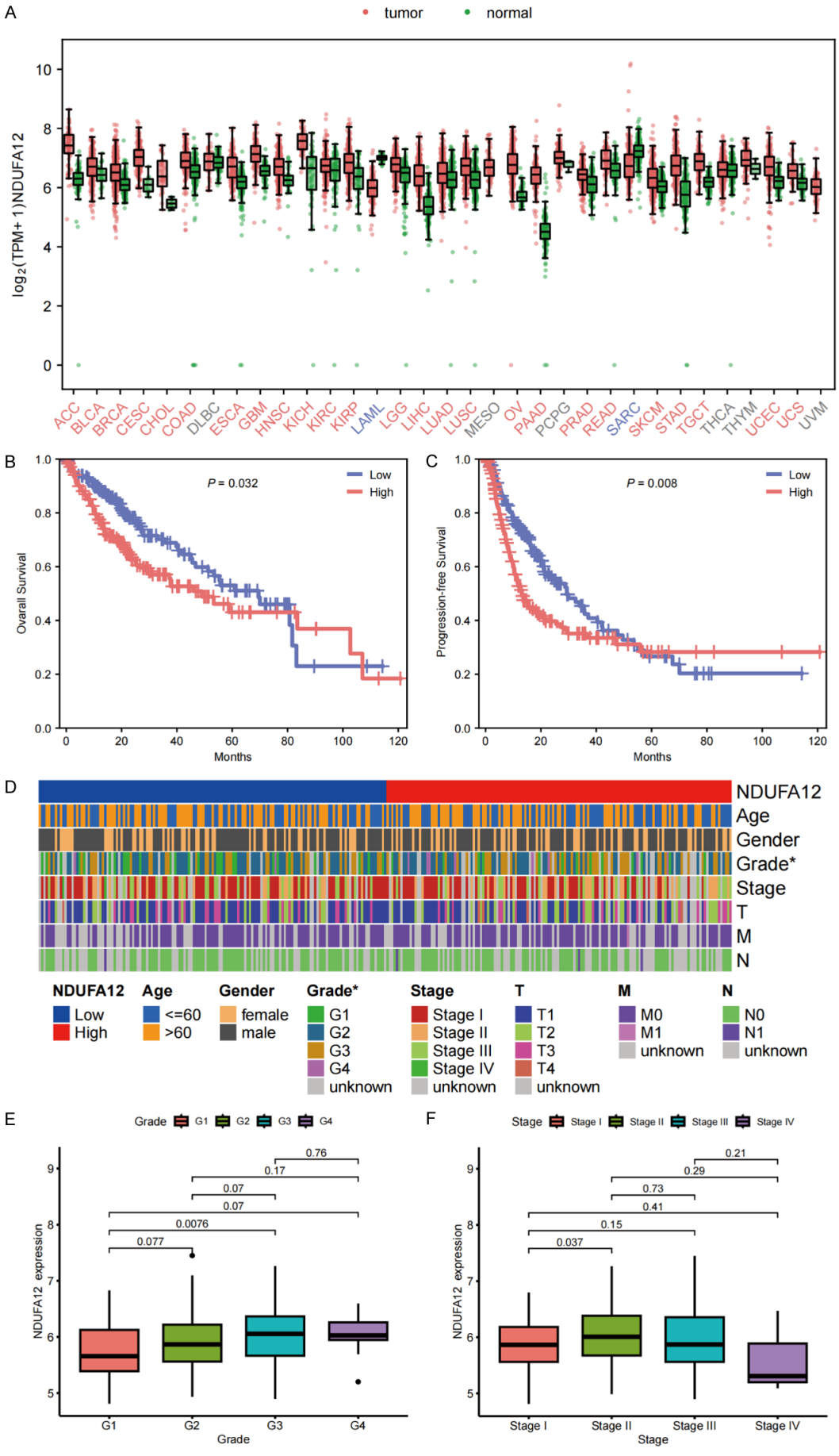
A
tumor
normal
log2(TPM+ 1)NDUFA12
ACC BLCA BRCA CESC CHOL COAD DLBC ESCA GBM HNSC KICH KIRC KIRP LAML LGG LIHC LUAD LUSC MESO OV PAAD PCPG PRAD READ SARC SKCM STAD TGCT THCA THYM UCEC UCS UVM
B
P = 0.032
Low
High
Overall Survival
Months
C
P = 0.008
Low
High
Progression-free Survival
Months
D
NDUFA12
Age
Gender
Grade*
Stage
T
M
N
NDUFA12 Low High
Age <=60 >60
Gender female male
Grade* G1 G2 G3 G4 unknown
Stage Stage I Stage II Stage III Stage IV unknown
T T1 T2 T3 T4 unknown
M M0 M1 unknown
N N0 N1 unknown
E
Grade G1 G2 G3 G4
NDUFA12 expression
0.076
0.17
0.07
0.07
0.0076
0.077
G1 G2 G3 G4
Grade
F
Stage Stage I Stage II Stage III Stage IV
NDUFA12 expression
0.21
0.29
0.73
0.41
0.15
0.037
Stage I Stage II Stage III Stage IV
Stage

Figure 1. Aberrant upregulation of NDUFA12 in pan-cancer and its prognostic significance in LIHC. A. Comparison of NDUFA12 expression between tumor and normal samples across pan-cancer types. B, C. Kaplan-Meier survival analyses of LIHC patients stratified by median NDUFA12 expression levels, demonstrating a significantly different OS and PFS of patients with high or low NDUFA12 expression levels. D. Distribution of clinicopathological features between high- and low-expression groups, indicating a significant difference in tumor grade. E. Association between NDUFA12 expression and tumor grade, showing a progressive increase in expression with higher histological grade. F. Correlation between NDUFA12 expression and clinical stage. *P < 0.05.

samples yielded the same results, with an upregulation of NDUFA12 expression in tumor samples (Figure S1). For patients with different expression levels, survival analyses demonstrated a significantly longer OS and PFS in the low-expression group in comparison with the high-expression group (median OS, 69.52 vs. 48.95 months, P = 0.032; median PFS, 29.34 vs. 13.08 months, P = 0.008) (**Figure 1B**, **1C**). With respect to clinicopathological features, tumor grade was significantly differentiated between two groups of patients (**Figure 1D**). Although a marked difference in NDUFA12 expression was observed only between grade 1 and grade 3 patients (P = 0.008), a trend of increasing expression with higher tumor grade was noted (**Figure 1E**). Besides, LIHC patients of stage II exhibited a notably higher NDUFA12 expression level compared to patients of stage I (P = 0.037) (**Figure 1F**).

Different NDUFA12 expression groups exhibit distinct DEG profiles and functional enrichment

Correlation analysis identified 30 genes that were strongly positively correlated with NDUFA12 expression according to the predefined threshold of Pearson R > 0.6 and P < 0.001 mentioned above. The six genes with the highest positive correlation coefficient (cor R) - *NDUFB4*, *UQCRH*, *NDUFS3*, *MRPL47*, *NDUFB3*, and *NUDT1* - were all mitochondria-related. For descriptive visualization, the top-ranked negatively correlated genes included *ADH1B*, *TTPA*, *CFHR4*, *SLC13A5*, *C8A*, and *SLC9B2*, were also illustrated in the circular plot (**Figure 2A**; Table S2). However, their absolute correlation coefficients did not exceed 0.6, and therefore they were interpreted only as exploratory features rather than strongly correlated genes. The associations between expression of NDUFA12 and NDUFB4 (cor R = 0.73), UQCRH (cor R = 0.68), NDUFS3 (cor R = 0.67), NDUFB3 (cor R = 0.66) were displayed (**Figure 2B-E**). A total of 168 genes were discovered to be differentially expressed between two expression groups. Briefly, 100 genes including *BEX2*, *MYBL2*, and *CDC20*, etc. were upregulated in the high group, while the remaining 68 genes including *CYP2E1*, *ADH4*, and *CYP3A4*, etc. were downregulated (**Figure 2F**). Regarding the results of functional enrichment, the most upregulated genes in the high group were enriched in nuclear division (BP, n = 37), chromosomal region (CC, n = 24), and tubulin binding (MF, n = 12) (**Figure 3A**). In contrast, downregulated genes were linked to steroid metabolic process (BP, n = 16), blood microparticle (CC, n = 8), and three MF terms - monooxygenase activity, iron ion binding, and oxidoreductase activity - each with 12 genes (**Figure 3B**). KEGG pathway enrichment analysis revealed that the cell cycle was the most enriched among upregulated pathways (**Figure 3C**), whereas the retinol metabolism was the leading pathways among downregulated ones (**Figure 3D**), conforming to the physiological functions of the liver.

The immune landscape and TMB vary across different NDUFA12 expression groups

The ESTIMATE algorithm showed that the low-expression group had markedly higher stromal (*P* = 0.008) and ESTIMATE (*P* = 0.035) scores, whereas the immune score was comparable between the two groups (**Figure 3E**). To be more precise, naïve B cells (*P* = 0.020) and resting natural killer (NK) cells (*P* = 0.006) were more infiltrated in the low-expression group, while memory B cells (*P* = 0.047), follicular helper T cells (*P* = 0.007), and Treg cells (*P* = 0.006) were more infiltrated in the high-expression group, suggesting transcriptomic differences related to NDUFA12-associated immune features. However, both memory B cells and resting NK cells constituted only a minor fraction of the immune infiltrate (**Figure 3F**). With respect to the correlation between NDUFA12 expression and immune cells, follicular helper T cells displayed the strongest positive correlation with NDUFA12 (cor R = 0.21; *P* < 0.001), whereas naïve B cells showed the strongest negative correlation (cor R = -0.17; *P* = 0.003)

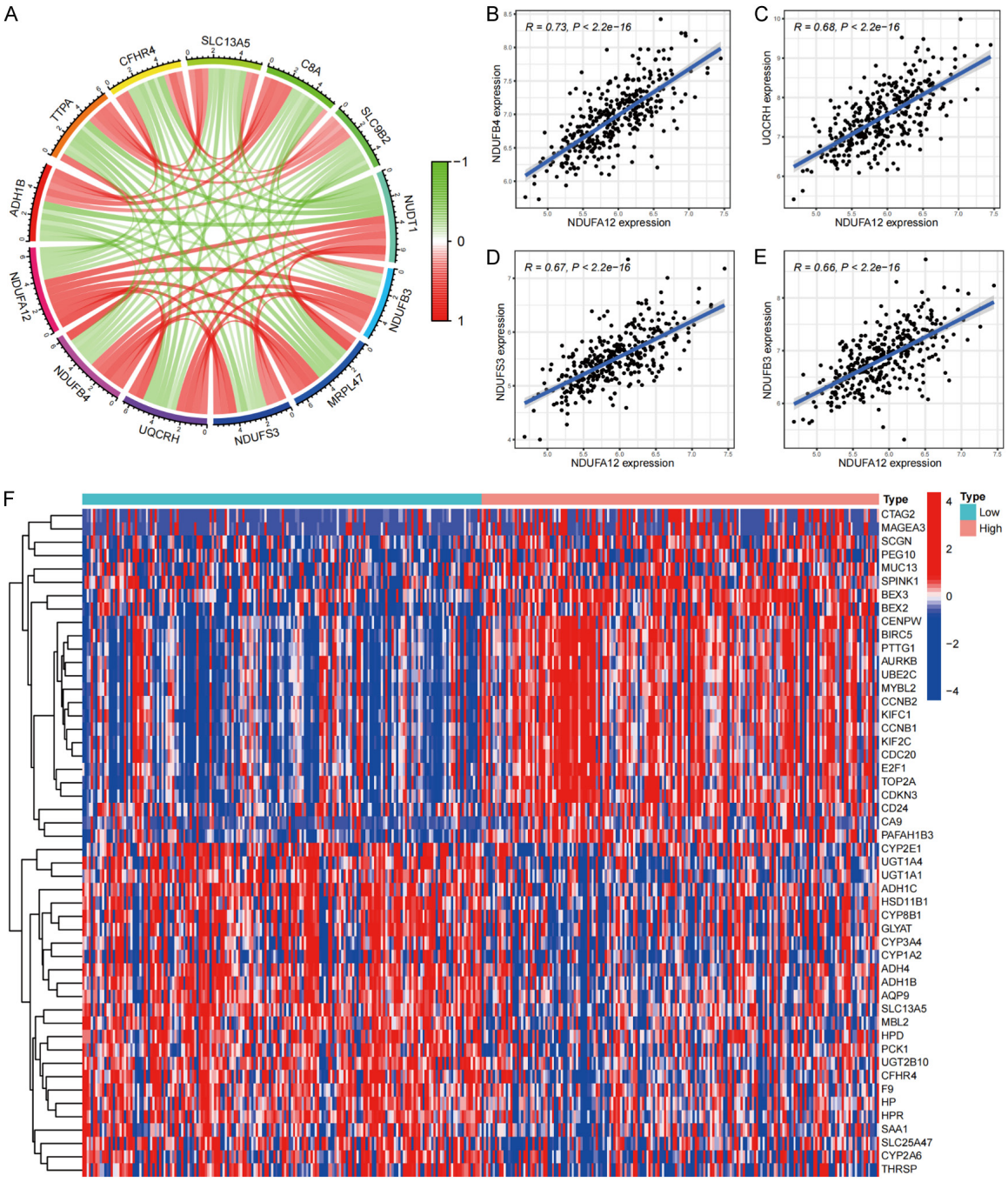

Figure 2. Distinct gene correlation patterns and differential expression profiles associated with NDUFA12 in LIHC. A. Circular plot showing genes correlated with NDUFA12 expression. The six strongest positively correlated genes meeting the predefined threshold of Pearson R > 0.6 and P < 0.001 included NDUFB4, UQCRH, NDUFS3, MRPL47, NDUFB3, and NUDT1. The top-ranked negatively correlated genes, including ADH1B, TTPA, CFHR4, SLC13A5, C8A, and SLC9B2, were also displayed for descriptive visualization. B-E. Scatter plots showing strong positive correlations between NDUFA12 and representative mitochondrial genes, including NDUFB4, UQCRH, NDUFS3, and NDUFB3. F. Heatmap depicting the top 25 upregulated and downregulated differentially expressed genes (DEGs) between high- and low-NDUFA12 expression groups.

(**Figure 4A**; Table S3). The TCIA-derived immune phenotype scoring featured the CTLA4(-)/PD1(-) cells were slightly increased in the low-expression group (P = 0.098) (**Figure 4B**).

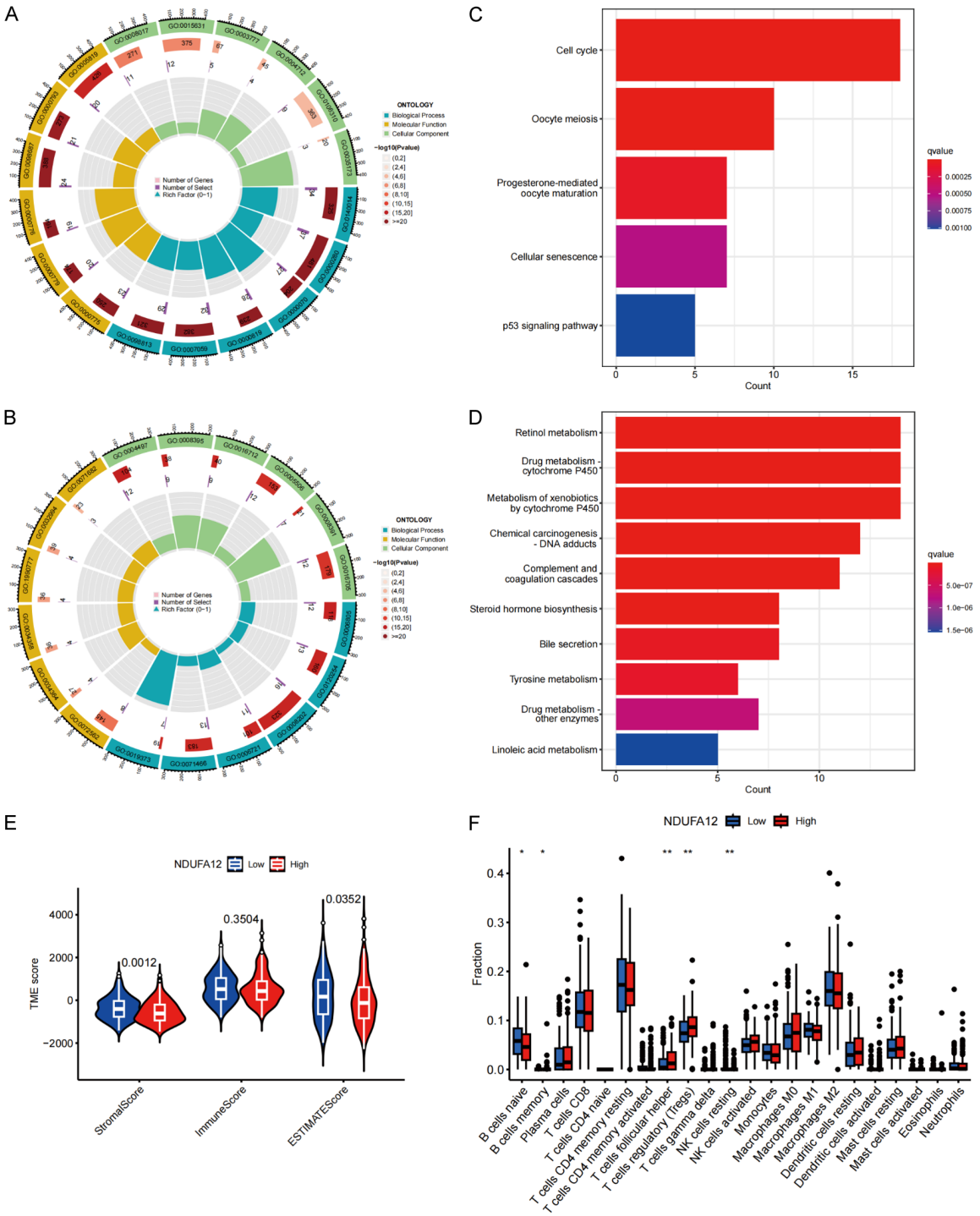

Figure 3. Functional enrichment and immune landscape differences between high- and low-NDUFA12 expression groups in LIHC. A, B. Gene Ontology (GO) enrichment analyses of differentially expressed genes (DEGs) between high- and low-NDUFA12 expression groups. C, D. KEGG pathway enrichment analyses of DEGs between high- and low-NDUFA12 expression groups. E. ESTIMATE analysis of the tumor microenvironment between two groups, including the stromal, immune and ESTIMATE scores. F. Comparison of immune cell infiltration profiles, demonstrating higher proportions of naïve B cells and resting NK cells in the low-expression group, and increased infiltration of memory B cells, follicular helper T cells, and Treg cells in the high-expression group. *P < 0.05, **P < 0.01.

Moreover, NDUFA12 indicated the strongest association with CD276 (cor R = 0.40; *P* < 0.001) (**Figure 4C**). The high-expression group also showed a higher TMB (*P* = 0.017) (**Figure**

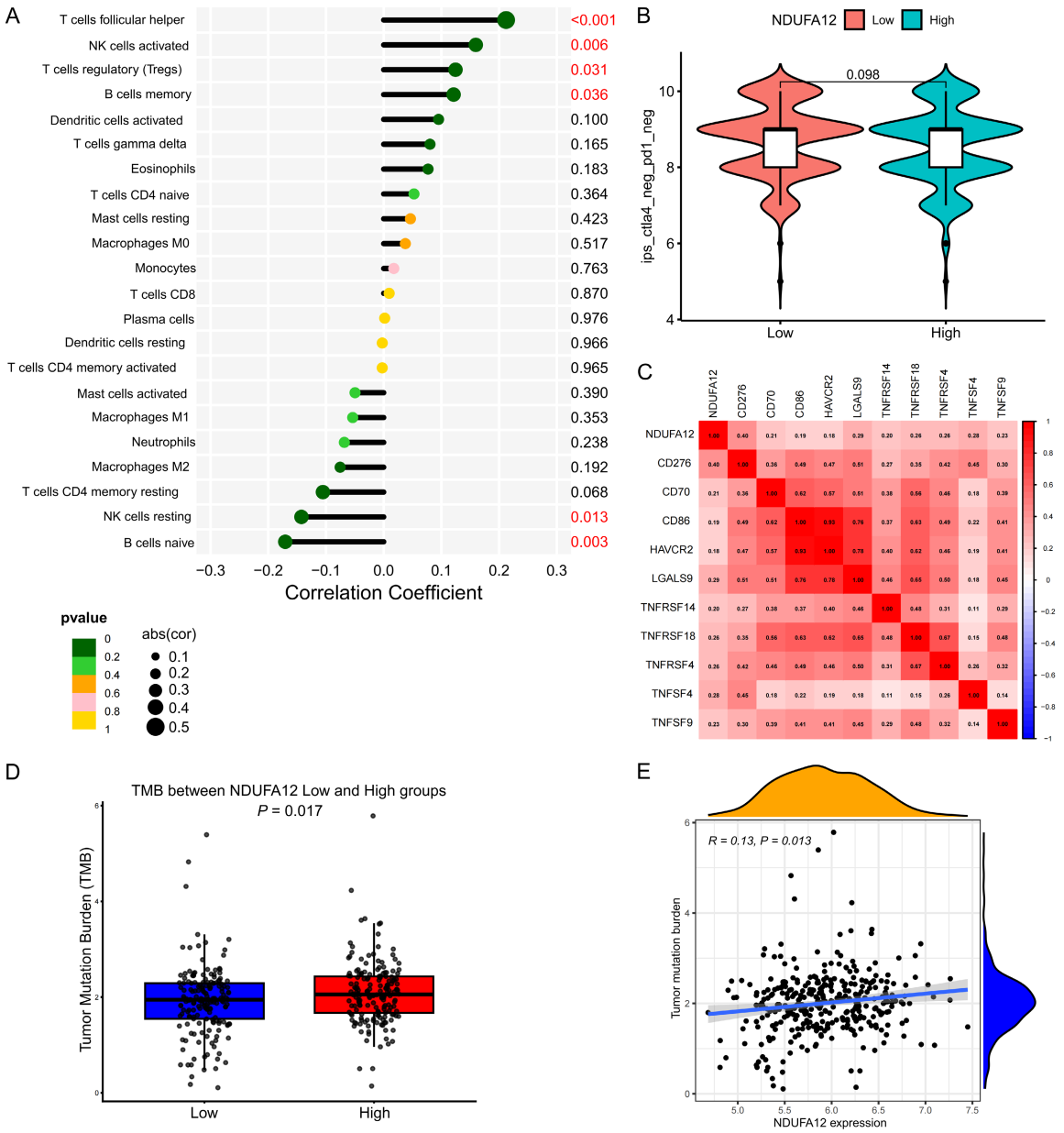

Figure 4. Association of NDUFA12 expression with immune infiltration, immune checkpoints, and TMB in LIHC. A. Correlation analysis between NDUFA12 expression and immune cell infiltration levels, showing the strongest positive correlation with follicular helper T cells and the strongest negative correlation with naïve B cells. B. Comparison of TCIA-derived specific immune phenotype cells between high- and low-expression groups, indicating a slight increase in the low-expression group. C. Correlation analysis between NDUFA12 and immune checkpoints. D. Comparison of tumor mutation burden (TMB) between groups, demonstrating significantly higher TMB in the high-expression group. E. The positive correlation between NDUFA12 expression and TMB.

4D), and NDUFA12 expression and TMB was unveiled to be positively associated (cor R = 0.13; *P* = 0.013) (**Figure 4E**).

NDUFA12 correlates with a relatively poor prognosis in our clinical cohort

The cohort from our hospital was composed of 25 patients including 1 female and 24 male patients. The average age of the cohort was 54.72 (10.41) years. All patients were HBV infected, and 7 patients had extrahepatic disease. The median AFP level [interquartile range (IQR)] was 45.42 [10.98, 2013.75]. For immunotherapy, 22 patients received a programmed cell death protein 1 (PD-1) inhibitor, while the left 3 patients received a programmed death-

Table 1. Baseline characteristics of 25 patients from our hospital

Characteristics	Level	Number (n, %)
Gender	Female	1 (4.0)
	Male	24 (96.0)
Age (mean (SD[a]))	-	54.72 (10.41)
HBV infection	-	25 (100.0)
AFP (median [IQR])	-	45.42 [10.98, 2013.75]
Extrahepatic disease	No	13 (52.0)
	Yes	7 (28.0)
	NA	5 (20.0)
ECOG	0	12 (48.0)
	1	8 (32.0)
	NA	5 (20.0)
Child Pugh	A	23 (92.0)
	B	1 (4.0)
	NA	1 (4.0)
BCLC	A	4 (16.0)
	B	5 (20.0)
	C	11 (44.0)
	NA	5 (20.0)
Immunotherapy	PD-1 inhibitor	22 (88.0)
	PD-L1 inhibitor	3 (12.0)
Targeted therapy	TKI	18 (72.0)
	Bevacizumab	7 (28.0)
Treatment lines	1	11 (44.0)
	2	14 (56.0)
BOR	CR	2 (8.0)
	PR	6 (24.0)
	SD[b]	13 (52.0)
	PD	4 (16.0)

Note: SD[a], standard deviation; IQR, interquartile range; ECOG, Eastern Cooperative Oncology Group; BCLC, Barcelona Clinic Liver Cancer; BOR, best overall response; PD-1, programmed cell death protein 1; PD-L1, programmed death-ligand 1; TKI, tyrosine kinase inhibitor; CR, complete response; PR, partial response; SD[b], stable disease; PD, progressive disease.

ligand 1 (PD-L1) inhibitor. For targeted-therapy, 18 patients received a TKI, whereas the remaining 7 received bevacizumab. The BORs of all patients including 2 complete response (CR), 6 partial response (PR), 13 stable disease (SD) and 4 progressive disease (PD) (**Table 1**). In our cohort, the objective response rate (ORR) was 32%, while the disease control rate (DCR) was 84%. As of November 1, 2024, the median follow-up time was 23.02 [21.34, NA] months. The median PFS (mPFS) was 14.1 months (**Figure 5A**), and the median OS (mOS) was 22.95 months (**Figure 5B**). Then, the cohort was stratified into high- and low-expression groups based on the median NDUFA12 value. Both PFS (**Figure 5C**) and OS (**Figure 5D**) tended to be longer in patients with low NDUFA12 expression than in those with high NDUFA12 expression, although the differences did not reach statistical significance (PFS, P = 0.24; OS, P = 0.094). In terms of DCR and ORR, the two expression groups are comparable with each other (**Figure 5E**). The CIBERSORT algorithm was again conducted using the RNA-sequencing results, as mentioned above. The follicular helper T cells were confirmed to be positively and significantly correlated with NDUFA12 expression (cor R = 0.48; P = 0.025), even though the memory B cells and Treg cells were not significantly correlated (**Figure 5F**). Moreover, the notable negative correlation between resting NK cells and NDUFA12 expression (cor R = -0.63; P < 0.001) was validated in our cohort (**Figure 5F**; **Table 2**).

NDUFA12 promotes the proliferation, migration, and invasion of liver cancer cells

NDUFA12 knockdown in MHCC-97H and PLC/PRF/5 cells was validated by qPCR and western blotting. Results showed that NDUFA12 was significantly downregulated in both cell lines at RNA and protein levels (**Figure 6A**, **6B**). The siNDUFA12-1 and siNDUFA12-3 sequences were used for further experiments. The CCK8 assay demonstrated that the proliferation of MHCC-97H and PLC/PRF/5 cells was significantly inhibited by NDUFA12 knockdown (**Figure 6C**). The EdU results further confirmed the repressed cell growth of MHCC-97H and PLC/PRF/5 cells with downregulated expression of NDUFA12 (**Figure 6D**). Then the invasion and migration ability was measured. A shorter migration distance at 24 h was observed in MHCC-97H and PLC/PRF/5 cells with NDUFA12 knockdown, compared to the control group, as delineated by the wound healing assay (**Figure 6E**). The Transwell assay showed a smaller number of migrating and invading MHCC-97H and PLC/PRF/5 cells in the lower chamber

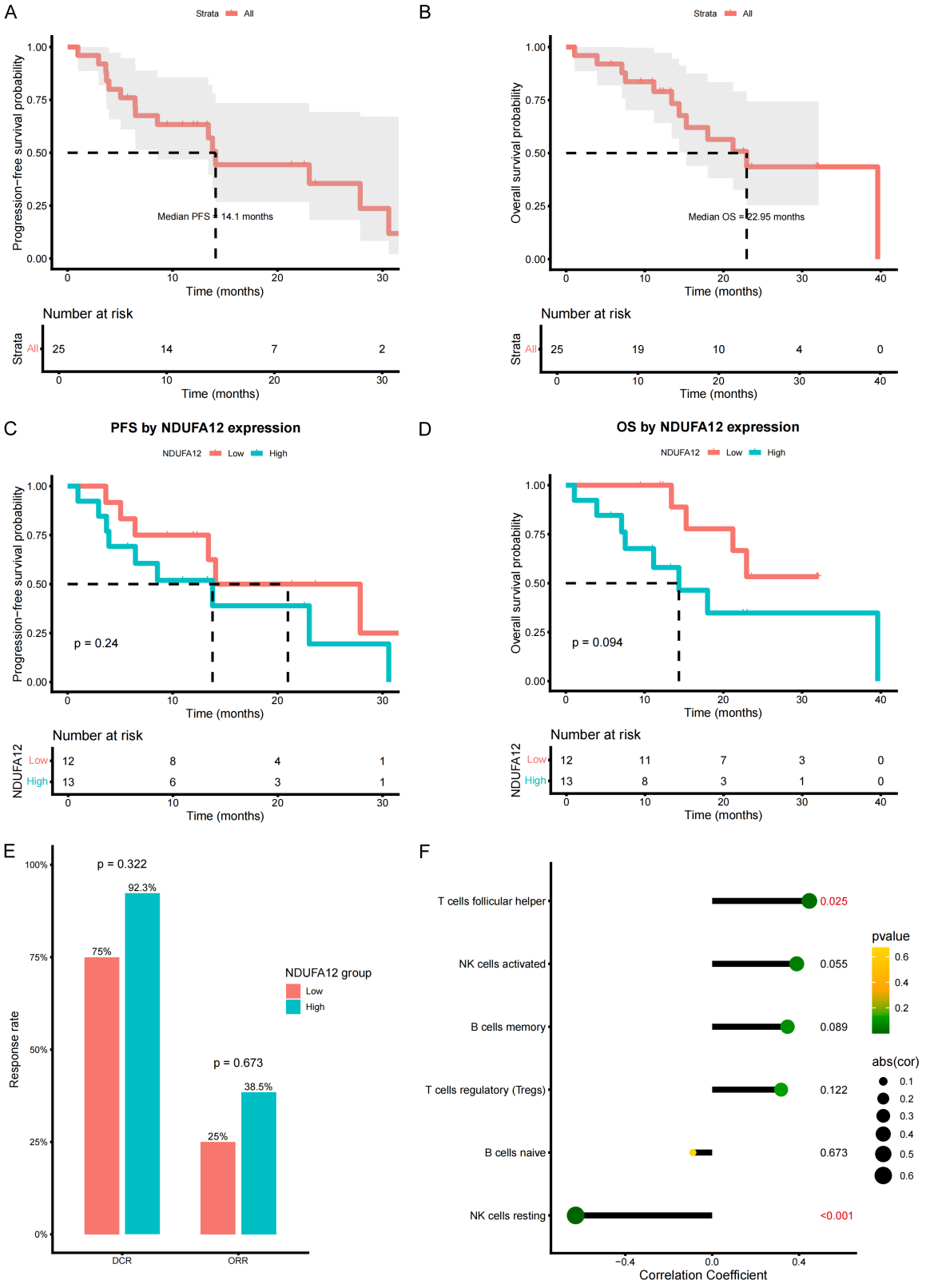

Figure 5. Survival outcomes and transcriptional characteristics according to NDUFA12 expression in advanced HCC patients from our cohort. (A, B) Kaplan-Meier survival analyses of PFS (A) and OS (B) in the entire cohort. (C, D) Kaplan-Meier survival analyses of PFS (C) and OS (D) between high- and low-NDUFA12 expression groups. (E) Comparison of DCR and ORR between high- and low-NDUFA12 expression groups. (F) Comparison of immune cell infiltration profiles, indicating a significantly positive correlation of high NDUFA12 expression with follicular helper T cells, along with a significantly negative correlation with resting NK cells.

Table 2. Correlation of NDUFA12 expression with immune cell infiltration estimated by the CIBERSORT algorithm in our cohort

Cell type	Correlation	*P*_value
NK cell resting	-0.628390802	0.000768643
B cell naive	-0.088803751	0.672935714
T cell regulatory	0.317548907	0.121909622
B cell memory	0.34696277	0.089272328
NK cell activated	0.389210742	0.054475989
T cell follicular helper	0.447368928	0.024941377

when NDUFA12 was downregulated (**Figure 6F**).

Knockdown of NDUFA12 alters energy metabolism of liver cancer cells

To further elucidate the role of NDUFA12 in regulating cellular energy metabolism in HCC cells, we systematically evaluated mitochondrial oxidative phosphorylation and glycolysis-related parameters in MHCC-97H and PLC/PRF/5 cells. Seahorse XF mitochondrial stress tests showed that NDUFA12 knockdown reduced the OCR in both cell lines, indicating impaired mitochondrial oxidative phosphorylation (**Figures 7A**, S2A-F). Further analysis of mitochondrial respiratory parameters revealed reductions in basal respiration, maximal respiration, ATP-linked respiration, and spare respiratory capacity after NDUFA12 knockdown. Consistent with the suppression of mitochondrial respiration, glycolysis stress tests showed that ECAR was increased after NDUFA12 knockdown, indicating enhanced glycolytic activity (**Figures 7B**, S2G-J). Quantitative analysis further showed that glycolysis and glycolytic capacity were significantly increased in MHCC-97H cells, with similar trends observed in PLC/PRF/5 cells.

We next evaluated ATP production and mitochondrial functional status. Cellular ATP levels were decreased after NDUFA12 knockdown (**Figure 7C**). Lactate assays further showed that lactate production was significantly increased in both MHCC-97H and PLC/PRF/5 cells following NDUFA12 knockdown compared with control cells (**Figure 7D**). Mitochondrial membrane potential staining revealed markedly reduced red fluorescence intensity in NDUFA12-silenced cells, indicating decreased mitochondrial membrane potential (**Figure 7E**). In addition, intracellular ROS detection showed that ROS levels were reduced after NDUFA12 knockdown (**Figure 7F**). These findings indicate that NDUFA12 knockdown suppresses mitochondrial oxidative phosphorylation in HCC cells, while increasing the ECAR and lactate production.

Discussion

Here, we systematically explored the expression profiles, prognostic value, and biological function of NDUFA12 in hepatocellular carcinoma. Our findings demonstrated that NDUFA12 was significantly upregulated in HCC samples and was closely associated with advanced tumor stage and unfavorable prognosis. Analyses of DEGs, immune infiltration, and TMB suggested that the NDUFA12 low-expression group exhibited a distinct immune infiltration pattern and lower TMB. A total of 25 patients treated with targeted-immunotherapy at our hospital were enrolled (Table S4). The RNA-sequencing assay of baseline tumor samples confirmed a longer overall survival in patients with low NDUFA12 expression. Functional experiments further confirmed that NDUFA12 knockdown suppressed proliferation, migration, and invasion, and altered cellular energy metabolism of HCC cells, suggesting that NDUFA12 may play a tumor-promoting role and serve as a candidate target of HCC treatment.

As one of the most prevalent cancers worldwide, HCC imposes a significant global burden. A substantial proportion of cases are detected at advanced stages, thus losing the opportunity for surgical resection [26]. Despite recent advances in systemic therapies for unresectable HCC, including immune checkpoint inhibitors combined with targeted therapy [27], therapeutic resistance and heterogeneous responses remain major challenges [28]. Therefore, identifying novel molecular markers and therapeutic targets is still of great clinical importance. In the present study, NDUFA12 was found to play a vital role in HCC, highlighting its potential value as a prognostic biomarker in HCC.

Mitochondrial dysfunction plays a role in various diseases, including nervous system diseases, metabolic syndromes [29], and cancers [30]. The modification of mitochondrial characteristics, such as oxidative damage, mitophagy dysregulation, mitochondrial dysregulation,

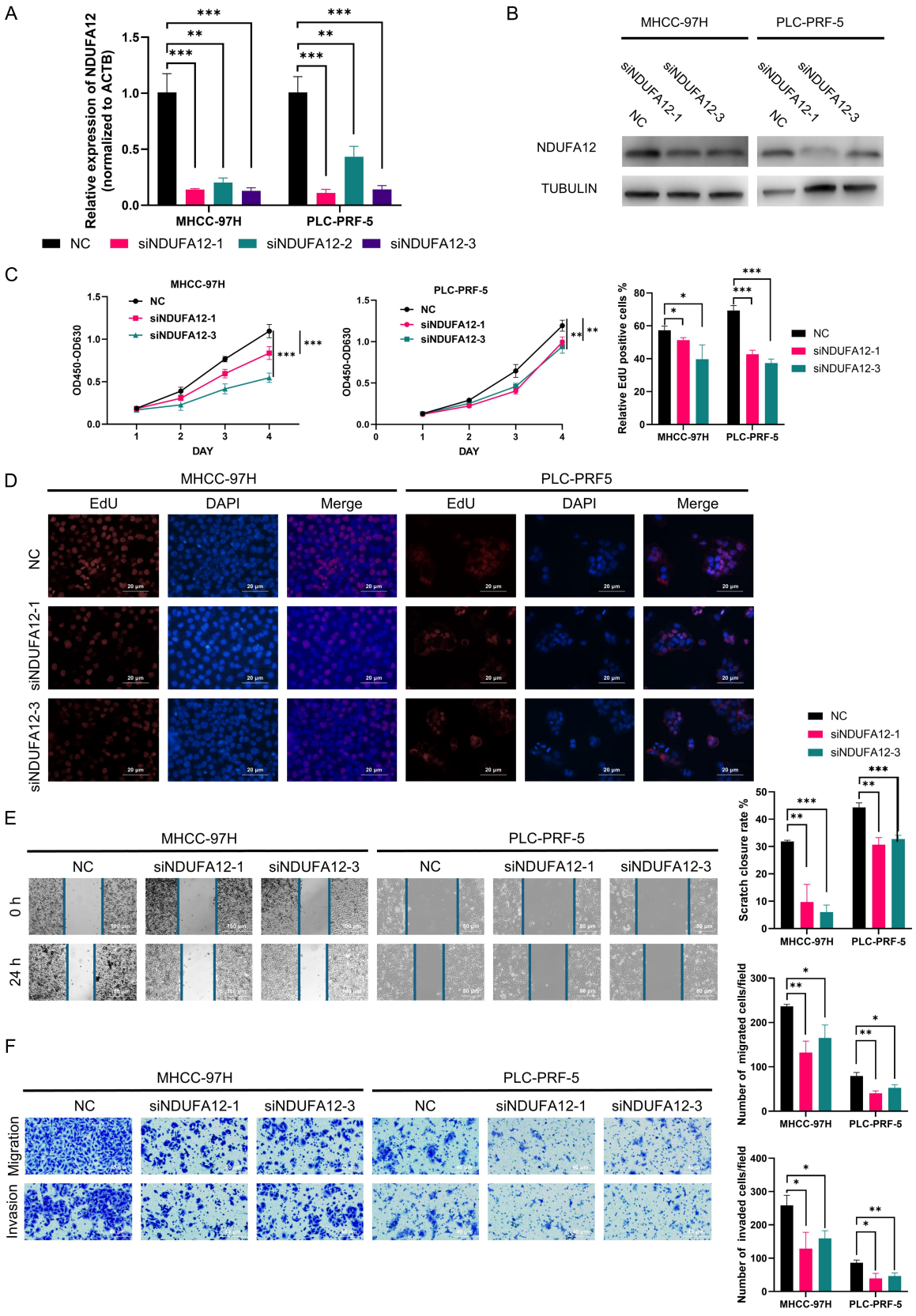

Figure 6. NDUFA12 knockdown inhibits proliferation, migration, and invasion in liver cancer cells. A, B. Validation of NDUFA12 knockdown efficiency in MHCC-97H and PLC/PRF/5 cells transfected with siNDUFA12, confirmed by qPCR and western blot analyses. C. CCK-8 assay showing significantly reduced proliferation of MHCC-97H and

PLC/PRF/5 cells following NDUFA12 knockdown. D. EdU assay confirmed the suppressed cell growth in NDUFA12-silenced cells. E. Wound healing assay demonstrating decreased migratory capacity in NDUFA12-knockdown cells at 24 h. F. Transwell migration and invasion assays revealing fewer migrated and invaded cells in the lower chamber upon NDUFA12 knockdown. Data are presented as the mean ± SD. *P < 0.05, **P < 0.01, ***P < 0.001; ns, not significant.

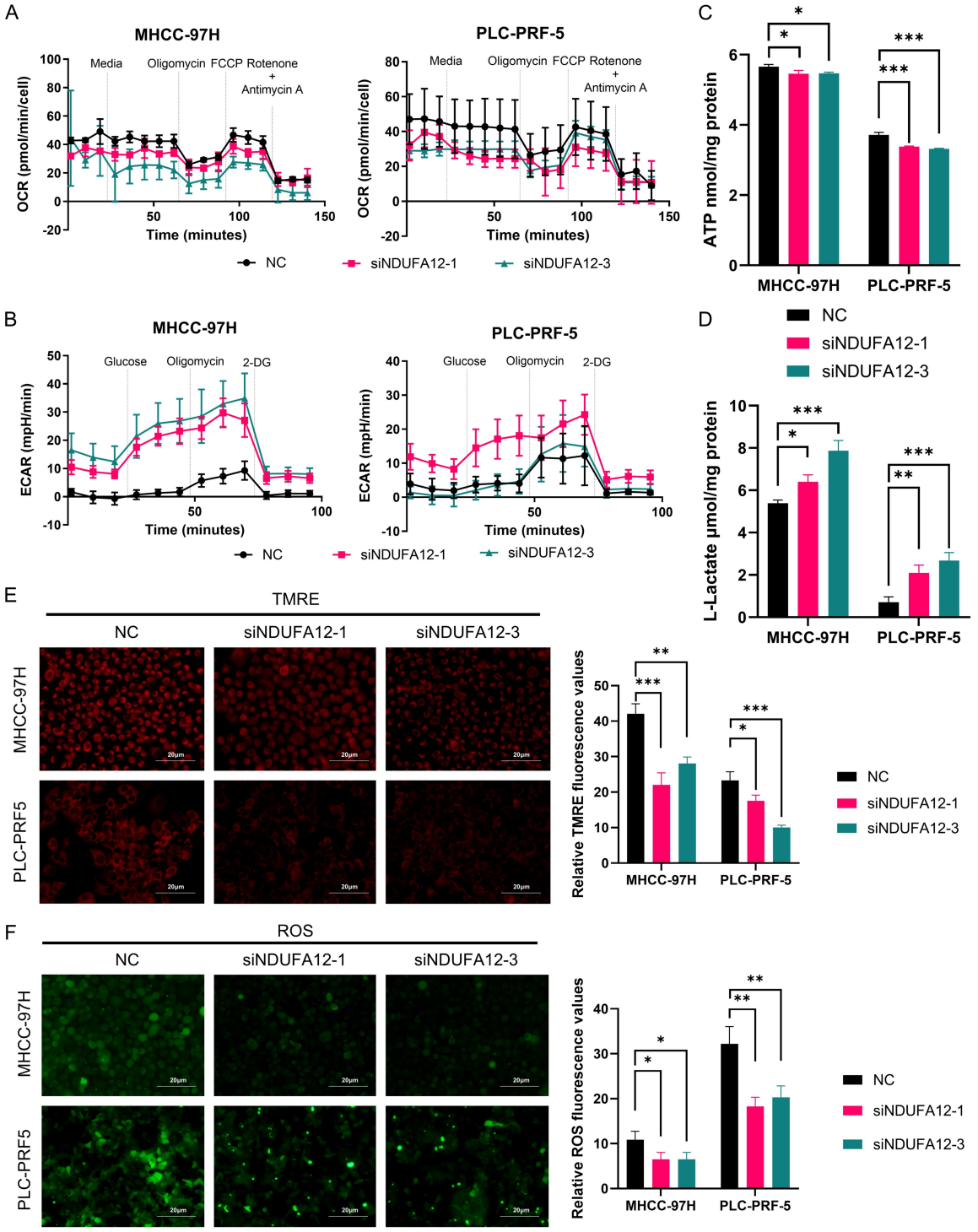

Figure 7. NDUFA12 knockdown induces mitochondrial metabolic alterations and compensatory glycolytic activation in HCC cells. A. Seahorse XF mitochondrial stress test showing OCR curves in MHCC-97H and PLC/PRF/5 cells after NDUFA12 knockdown. B. Seahorse XF glycolysis stress test showing ECAR curves in MHCC-97H and PLC/PRF/5

cells after NDUFA12 knockdown. C. Cellular ATP levels were decreased after NDUFA12 knockdown in both cell lines. D. Lactate production was increased following NDUFA12 knockdown in both cell lines. E. Representative mitochondrial membrane potential staining images and quantitative analysis showing reduced mitochondrial membrane potential in NDUFA12-silenced cells. F. Representative ROS fluorescence images and quantitative analysis showing decreased intracellular ROS levels after NDUFA12 knockdown. Data are presented as the mean ± SD. *P < 0.05, **P < 0.01, ***P < 0.001; ns, not significant.

and mitochondrial DNA (mtDNA) alteration, are likely to occur during cancer development [30, 31]. For example, a low mtDNA copy number has been reported as a significant predictor of large tumor size, liver cirrhosis, and reduced 5-year survival in HCC [32]. Besides, a number of studies have highlighted the critical role of oxidative damage in HCC progression. On the one hand, mitochondrial dysfunction induced by certain mtDNA mutations is known to promote reactive oxygen species overproduction [33], which might activate oncogenic pathways and/or increase genome instability [34]. However, numerous studies have disclosed the detrimental role of ROS in cell survival, and that the elimination of ROS could promote tumor progression. It was demonstrated that the improved mitochondrial function could mitigate excessive intracellular ROS, thus promoting HCC progression [35]. According to other studies, the intracellular mitochondrial ROS could be enhanced by sorafenib treatment, leading to ferroptosis in liver cancer cells [36, 37]. Therefore, it is interesting to see the dual effects of mitochondrial ROS in HCC progression, where a low or moderate level might potentially cause tumor progression via activation of oncogenic pathways, while a high level might contribute to ferroptosis, or other forms of mitochondria-related cell death [31, 37].

As a subunit of mitochondrial complex I, NDUFA12 participates in oxidative phosphorylation and cellular energy production. Studies focusing on Ertredin treatment indicated that NDUFA12 inhibition could suppress cancer cells, including HepG2 cells [15, 16]. Additionally, Song et al. reported that NDUFA12 downregulation suppressed oxidative phosphorylation, thereby shifting energy production to glycolysis and mitigating progression phenotypes of lung cancer cells [38]. Consistent with these observations, our functional experiments demonstrated that NDUFA12 knockdown impaired mitochondrial respiration in MHCC-97H and PLC/PRF/5 cells. Expanded metabolic analyses further showed that NDUFA12 silencing reduced multiple OCR-related parameters, including basal respiration, etc., accompanied by decreased ATP production and mitochondrial membrane potential. In contrast, ECAR and lactate production were increased after NDUFA12 knockdown, suggesting a compensatory activation of glycolysis. Notably, intracellular ROS levels were also reduced, which may reflect decreased mitochondrial electron transport activity and overall electron flux under suppressed respiratory conditions. Together, these findings indicate that NDUFA12 downregulation induces a metabolic alteration characterized by attenuated oxidative phosphorylation and enhanced glycolytic activity in HCC cells.

From a clinical perspective, our results further suggest that NDUFA12 may have potential value as a prognostic biomarker in HCC. Patients with lower NDUFA12 expression tended to exhibit a longer OS in both public database analyses and our cohort. Moreover, immune deconvolution analyses indicated that NDUFA12 expression was associated with distinct immune-related transcriptomic features. Nevertheless, the immune infiltration analyses in this study were mainly based on transcriptomic algorithms, including ESTIMATE, CIBERSORT, and TCIA-derived analyses. Although these approaches provide useful insights into immune-related features associated with NDUFA12 expression, they cannot replace direct histological or spatial validation. Future studies using larger cohorts with sufficient tissue availability should incorporate immunohistochemistry, multiplex immunofluorescence, or spatial transcriptomic analyses to further validate these findings.

Nevertheless, several limitations of this study should be acknowledged. For example, although in vitro functional assays confirmed the role of NDUFA12 in regulating malignant phenotypes of HCC cells, the precise molecular mechanisms underlying its effects remain unclear. Intriguingly, whether NDUFA12 knockdown induces mitophagy or ferroptosis is worthy of exploration, which might serve as the

downstream target. Future studies should focus on the downstream pathways of NDUFA12 and its role in animal models and clinical samples.

Conclusion

This study demonstrated that NDUFA12 is upregulated in hepatocellular carcinoma and is associated with poor prognosis and aggressive tumor phenotypes. Functional experiments indicated that NDUFA12 knockdown suppressed malignant phenotypes and induced mitochondrial metabolic alterations, characterized by reduced oxidative phosphorylation, decreased ATP production and mitochondrial membrane potential, and compensatory glycolytic activation in HCC cells. These findings indicate that NDUFA12 may function as a potential prognostic biomarker and candidate treatment target in HCC. We believe that further mechanistic investigations and clinical studies are warranted to fully define its role in hepatocellular carcinoma progression.

Acknowledgements

This study was funded by National Natural Science Foundation of China (Grant Nos. 81-972311 & 82141127), National Key Research and Development Program of China (2023YFC3403800, 2023YFC3403804), CAMS Innovation Fund for Medical Sciences (CIFMS) (2021-I2M-C&T-B-057), CAMS Innovation Fund for Medical Sciences (Grant No. 2021-I2M-1-066), and the CAMS Initiative for Innovative Medicine (Grant No. 2021-I2M-1-015).

Informed consent forms were signed and provided by all patients.

Disclosure of conflict of interest

None.

Address correspondence to: Jianqiang Cai and Hong Zhao, Department of Hepatobiliary Surgery, State Key Laboratory of Molecular Oncology, Beijing Key Laboratory of Cell and Gene Therapy for Digestive System Tumor, Key Laboratory of Gene Editing Screening and Research and Development of Digestive System Tumor Drugs (CAMS), National Cancer Center/National Clinical Research Center for Cancer/Cancer Hospital, Chinese Academy of Medical Sciences and Peking Union Medical College, No. 17 South Panjiayuan, Chaoyang District, Beijing 100021, China. E-mail: caijianqiang@cicams.ac.cn (JQC); zhaohong@cicams.ac.cn (HZ)

References

[1] Bray F, Laversanne M, Sung H, Ferlay J, Siegel RL, Soerjomataram I and Jemal A. Global cancer statistics 2022: GLOBOCAN estimates of incidence and mortality worldwide for 36 cancers in 185 countries. CA Cancer J Clin 2024; 74: 229-263.

[2] Han B, Zheng R, Zeng H, Wang S, Sun K, Chen R, Li L, Wei W and He J. Cancer incidence and mortality in China, 2022. J Natl Cancer Cent 2024; 4: 47-53.

[3] Cheng AL, Qin S, Ikeda M, Galle PR, Ducreux M, Kim TY, Lim HY, Kudo M, Breder V, Merle P, Kaseb AO, Li D, Verret W, Ma N, Nicholas A, Wang Y, Li L, Zhu AX and Finn RS. Updated efficacy and safety data from IMbrave150: atezolizumab plus bevacizumab vs. sorafenib for unresectable hepatocellular carcinoma. J Hepatol 2022; 76: 862-873.

[4] Ren Z, Xu J, Bai Y, Xu A, Cang S, Du C, Li Q, Lu Y, Chen Y, Guo Y, Chen Z, Liu B, Jia W, Wu J, Wang J, Shao G, Zhang B, Shan Y, Meng Z, Wu J, Gu S, Yang W, Liu C, Shi X, Gao Z, Yin T, Cui J, Huang M, Xing B, Mao Y, Teng G, Qin Y, Wang J, Xia F, Yin G, Yang Y, Chen M, Wang Y, Zhou H and Fan J; ORIENT-32 study group. Sintilimab plus a bevacizumab biosimilar (IBI305) versus sorafenib in unresectable hepatocellular carcinoma (ORIENT-32): a randomised, open-label, phase 2-3 study. Lancet Oncol 2021; 22: 977-990.

[5] Jiang Z, Fang Z, Hong D and Wang X. Cancer immunotherapy with "vascular-immune" crosstalk as entry point: associated mechanisms, therapeutic drugs and nano-delivery systems. Int J Nanomedicine 2024; 19: 7383-7398.

[6] Lee WS, Yang H, Chon HJ and Kim C. Combination of anti-angiogenic therapy and immune checkpoint blockade normalizes vascular-immune crosstalk to potentiate cancer immunity. Exp Mol Med 2020; 52: 1475-1485.

[7] Rui L. Energy metabolism in the liver. Compr Physiol 2014; 4: 177-197.

[8] Lee HY, Nga HT, Tian J and Yi HS. Mitochondrial metabolic signatures in hepatocellular carcinoma. Cells 2021; 10: 1901.

[9] Sharafi F, Rismani E, Rhmanian M, Khosravi A, Zarrabi A and Vosough M. Mitochondrial dysfunction in hepatocellular carcinoma: from metabolism to targeted therapies. Mol Cell Biochem 2025; 480: 6015-6038.

[10] Dieteren CE, Willems PH, Vogel RO, Swarts HG, Fransen J, Roepman R, Crienen G, Smeitink JA, Nijtmans LG and Koopman WJ. Subunits of mi-

tochondrial complex I exist as part of matrix- and membrane-associated subcomplexes in living cells. J Biol Chem 2008; 283: 34753-34761.
[11] Rak M and Rustin P. Supernumerary subunits NDUFA3, NDUFA5 and NDUFA12 are required for the formation of the extramembrane arm of human mitochondrial complex I. FEBS Lett 2014; 588: 1832-1838.
[12] Adjobo-Hermans MJW, de Haas R, Willems PHGM, Wojtala A, van Emst-de Vries SE, Wagenaars JA, van den Brand M, Rodenburg RJ, Smeitink JAM, Nijtmans LG, Sazanov LA, Wieckowski MR and Koopman WJH. NDUFS4 deletion triggers loss of NDUFA12 in Ndufs4$^{-/-}$ mice and Leigh syndrome patients: a stabilizing role for NDUFAF2. Biochim Biophys Acta Bioenerg 2020; 1861: 148213.
[13] Ostergaard E, Rodenburg RJ, van den Brand M, Thomsen LL, Duno M, Batbayli M, Wibrand F and Nijtmans L. Respiratory chain complex I deficiency due to NDUFA12 mutations as a new cause of Leigh syndrome. J Med Genet 2011; 48: 737-740.
[14] Torraco A, Nasca A, Verrigni D, Pennisi A, Zaki MS, Olivieri G, Assouline Z, Martinelli D, Maroofian R, Rizza T, Di Nottia M, Invernizzi F, Lamantea E, Longo D, Houlden H, Prokisch H, Rötig A, Dionisi-Vici C, Bertini E, Ghezzi D, Carrozzo R and Diodato D. Novel NDUFA12 variants are associated with isolated complex I defect and variable clinical manifestation. Hum Mutat 2021; 42: 699-710.
[15] Park SI, Cho SM, Atsumi S, Kawada M, Shibuya M, Lee JY, Kim JY and Kwon HJ. NDUFA12 as a functional target of the anticancer compound Ertredin in human hepatoma cells as revealed by label-free chemical proteomics. J Proteome Res 2024; 23: 130-141.
[16] Atsumi S, Nosaka C, Onodera T, Adachi H, Watanabe T, Kawada M, Shibuya M, Park SI and Kwon HJ. Enhanced anticancer activity of 7MeERT over Ertredin: a comparative study on cancer cell proliferation and NDUFA12 binding. Biomolecules 2024; 14: 1197.
[17] Kang YJ, Pan L, Liu Y, Rong Z, Liu J and Liu F. GEPIA3: enhanced drug sensitivity and interaction network analysis for cancer research. Nucleic Acids Res 2025; 53: W283-W290.
[18] Ritchie ME, Phipson B, Wu D, Hu Y, Law CW, Shi W and Smyth GK. Limma powers differential expression analyses for RNA-sequencing and microarray studies. Nucleic Acids Res 2015; 43: e47.
[19] Wu T, Hu E, Xu S, Chen M, Guo P, Dai Z, Feng T, Zhou L, Tang W, Zhan L, Fu X, Liu S, Bo X and Yu G. clusterProfiler 4.0: a universal enrichment tool for interpreting omics data. Innovation (Camb) 2021; 2: 100141.
[20] Gu Z, Eils R and Schlesner M. Complex heatmaps reveal patterns and correlations in multidimensional genomic data. Bioinformatics 2016; 32: 2847-2849.
[21] Gu Z, Gu L, Eils R, Schlesner M and Brors B. Circlize implements and enhances circular visualization in R. Bioinformatics 2014; 30: 2811-2812.
[22] Yoshihara K, Shahmoradgoli M, Martínez E, Vegesna R, Kim H, Torres-Garcia W, Treviño V, Shen H, Laird PW, Levine DA, Carter SL, Getz G, Stemke-Hale K, Mills GB and Verhaak RG. Inferring tumour purity and stromal and immune cell admixture from expression data. Nat Commun 2013; 4: 2612.
[23] Chen B, Khodadoust MS, Liu CL, Newman AM and Alizadeh AA. Profiling tumor infiltrating immune cells with CIBERSORT. Methods Mol Biol 2018; 1711: 243-259.
[24] Charoentong P, Finotello F, Angelova M, Mayer C, Efremova M, Rieder D, Hackl H and Trajanoski Z. Pan-cancer immunogenomic analyses reveal genotype-immunophenotype relationships and predictors of response to checkpoint blockade. Cell Rep 2017; 18: 248-262.
[25] Mayakonda A, Lin DC, Assenov Y, Plass C and Koeffler HP. Maftools: efficient and comprehensive analysis of somatic variants in cancer. Genome Res 2018; 28: 1747-1756.
[26] Kim E and Viatour P. Hepatocellular carcinoma: old friends and new tricks. Exp Mol Med 2020; 52: 1898-1907.
[27] Yang X, Yang C, Zhang S, Geng H, Zhu AX, Bernards R, Qin W, Fan J, Wang C and Gao Q. Precision treatment in advanced hepatocellular carcinoma. Cancer Cell 2024; 42: 180-197.
[28] Zhao Y, Zhang YN, Wang KT and Chen L. Lenvatinib for hepatocellular carcinoma: from preclinical mechanisms to anti-cancer therapy. Biochim Biophys Acta Rev Cancer 2020; 1874: 188391.
[29] Zong Y, Li H, Liao P, Chen L, Pan Y, Zheng Y, Zhang C, Liu D, Zheng M and Gao J. Mitochondrial dysfunction: mechanisms and advances in therapy. Signal Transduct Target Ther 2024; 9: 124.
[30] Al-Faze R, Ahmed HA, El-Atawy MA, Zagloul H, Alshammari EM, Jaremko M, Emwas AH, Nabil GM and Hanna DH. Mitochondrial dysfunction route as a possible biomarker and therapy target for human cancer. Biomed J 2025; 48: 100714.
[31] Hsu CC, Lee HC and Wei YH. Mitochondrial DNA alterations and mitochondrial dysfunction in the progression of hepatocellular carcinoma. World J Gastroenterol 2013; 19: 8880-8886.

[32] Yamada S, Nomoto S, Fujii T, Kaneko T, Takeda S, Inoue S, Kanazumi N and Nakao A. Correlation between copy number of mitochondrial DNA and clinico-pathologic parameters of hepatocellular carcinoma. Eur J Surg Oncol 2006; 32: 303-307.

[33] Vives-Bauza C, Gonzalo R, Manfredi G, Garcia-Arumi E and Andreu AL. Enhanced ROS production and antioxidant defenses in cybrids harbouring mutations in mtDNA. Neurosci Lett 2006; 391: 136-141.

[34] Park JS, Sharma LK, Li H, Xiang R, Holstein D, Wu J, Lechleiter J, Naylor SL, Deng JJ, Lu J and Bai Y. A heteroplasmic, not homoplasmic, mitochondrial DNA mutation promotes tumorigenesis via alteration in reactive oxygen species generation and apoptosis. Hum Mol Genet 2009; 18: 1578-1589.

[35] Li Z, Zhou H, Zhai X, Gao L, Yang M, An B, Xia T, Du G, Li X, Wang W and Jin B. MELK promotes HCC carcinogenesis through modulating cuproptosis-related gene DLAT-mediated mitochondrial function. Cell Death Dis 2023; 14: 733.

[36] Li Y, Xia J, Shao F, Zhou Y, Yu J, Wu H, Du J and Ren X. Sorafenib induces mitochondrial dysfunction and exhibits synergistic effect with cysteine depletion by promoting HCC cells ferroptosis. Biochem Biophys Res Commun 2021; 534: 877-884.

[37] Liu X, Liu T, Zhou Z, Bian K, Qiu C and Zhang F. Brusatol improves the efficacy of sorafenib in Huh7 cells via ferroptosis resistance dependent Nrf2 signaling pathway. Biochem Biophys Res Commun 2024; 734: 150762.

[38] Song Y, Zhu Z, Li H, Song S and Lin X. An immune cell activation signature for non - small cell lung cancer revealed tumor microenvironment heterogeneity and the role of RORA in regulating ZNF490/NDUFA12 axis. Curr Med Chem 2026; [Epub ahead of print].

Table S1. Primer sequences

	Sequence
siNDUFA12-1	sense 5'-CCUUAUUCUACCACUAGAATT-3'; antisense 5'-UUCUAGUGGUAGAAUAAGGTT-3'
siNDUFA12-2	sense 5'-GACUGAUGAUCCUCCAACATT-3'; antisense 5'-UGUUGGAGGAUCAUCAGUCTT-3'
siNDUFA12-3	sense 5'-CGAUGGGUUGUAUAUACUATT-3'; antisense 5'-UAGUAUAUACAACCCAUCGTT-3'
NDUFA12-NC	sense 5'-UUCUCCGAACGUGUCACGU-3'; antisense 5'-ACGUGACACGUUCGGAGAA-3'
NDUFA12 primer	forward 5'-CTGCCACTCTATGAGCTTAAGA-3'; reverse 5'-TATCCCTGCTTGCACATCTC-3'
ACTB primer	forward 5'-AGAGCTACGAGCTGCCTGAC-3'; reverse 5'-AGCACTGTGTTGGCGTACAG-3'

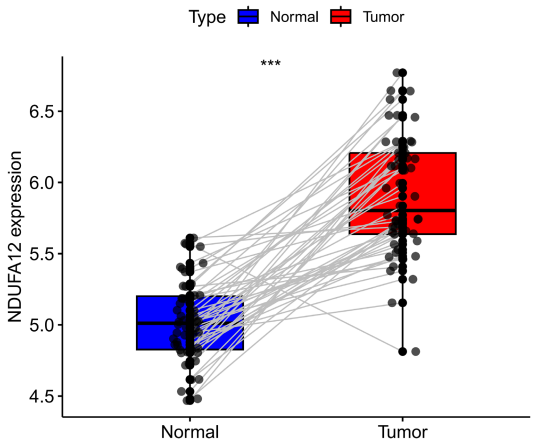

Figure S1. The NDUFA12 expression between paired tumor and normal samples in LIHC patients from TCGA database. Paired comparison of NDUFA12 expression between tumor and matched adjacent normal samples in LIHC patients from the TCGA database. Each gray line connects paired normal and tumor tissues from the same patient. NDUFA12 expression was significantly higher in tumor tissues than in matched normal tissues. ***P < 0.001.

Table S2. Gene correlation test found 30 genes significantly associated with NDUFA12 expression

Gene	Correlation	*P* value
ANAPC7	0.621569511	3.53E-40
ARPC3	0.627766767	3.53E-41
ATP5F1C	0.651949848	2.64E-45
ATP5MC2	0.652632673	1.99E-45
BOLA3	0.628780469	2.41E-41
C18orf21	0.60430557	1.65E-37
CCDC59	0.60510959	1.25E-37
COX5A	0.63394975	3.37E-42
COX8A	0.601407871	4.46E-37
GGCT	0.606680905	7.24E-38
GTF2A2	0.610302157	2.03E-38
MCRS1	0.616499271	2.23E-39
MRPL47	0.655477975	6.14E-46
NABP2	0.604284693	1.66E-37
NDUFB3	0.655054111	7.32E-46
NDUFB4	0.728873072	2.31E-61
NDUFS3	0.67128618	6.93E-49
NUDT1	0.654350877	9.81E-46
PA2G4	0.632026532	7.04E-42
PYM1	0.6123658	9.80E-39
RFC2	0.627211507	4.35E-41
RFC4	0.608161964	4.32E-38
SLC25A3	0.649838184	6.27E-45
SNRPF	0.624566867	1.17E-40
SNRPG	0.630876725	1.09E-41
TIMM50	0.605504969	1.09E-37
TPRKB	0.601469798	4.37E-37
UBE2M	0.601153813	4.87E-37
UQCRH	0.680105012	1.31E-50
VPS29	0.640681158	2.46E-43

Table S3. The correlation between NDUFA12 expression and immune cells

Cell	Correlation	*P* value
B cells naive	-0.170549197	0.0029937
B cells memory	0.121155926	0.035643052
Plasma cells	0.001740267	0.976013701
T cells CD8	0.009488481	0.869780157
T cells CD4 naive	0.052491984	0.364122105
T cells CD4 memory resting	-0.10531734	0.068051963
T cells CD4 memory activated	-0.002526746	0.965179346
T cells follicular helper	0.212117233	0.000209683
T cells regulatory (Tregs)	0.124454522	0.030879631
T cells gamma delta	0.080246218	0.164933872
NK cells resting	-0.142517342	0.013325795
NK cells activated	0.159597879	0.005516623
Monocytes	0.017485904	0.762553004
Macrophages M0	0.037532985	0.516537366
Macrophages M1	-0.053694748	0.353015265
Macrophages M2	-0.075462806	0.191560105
Dendritic cells resting	-0.002464495	0.966036701
Dendritic cells activated	0.095099679	0.099601814
Mast cells resting	0.046362196	0.422877925
Mast cells activated	-0.049673138	0.390483297
Eosinophils	0.076875337	0.183466533
Neutrophils	-0.068199038	0.238135491

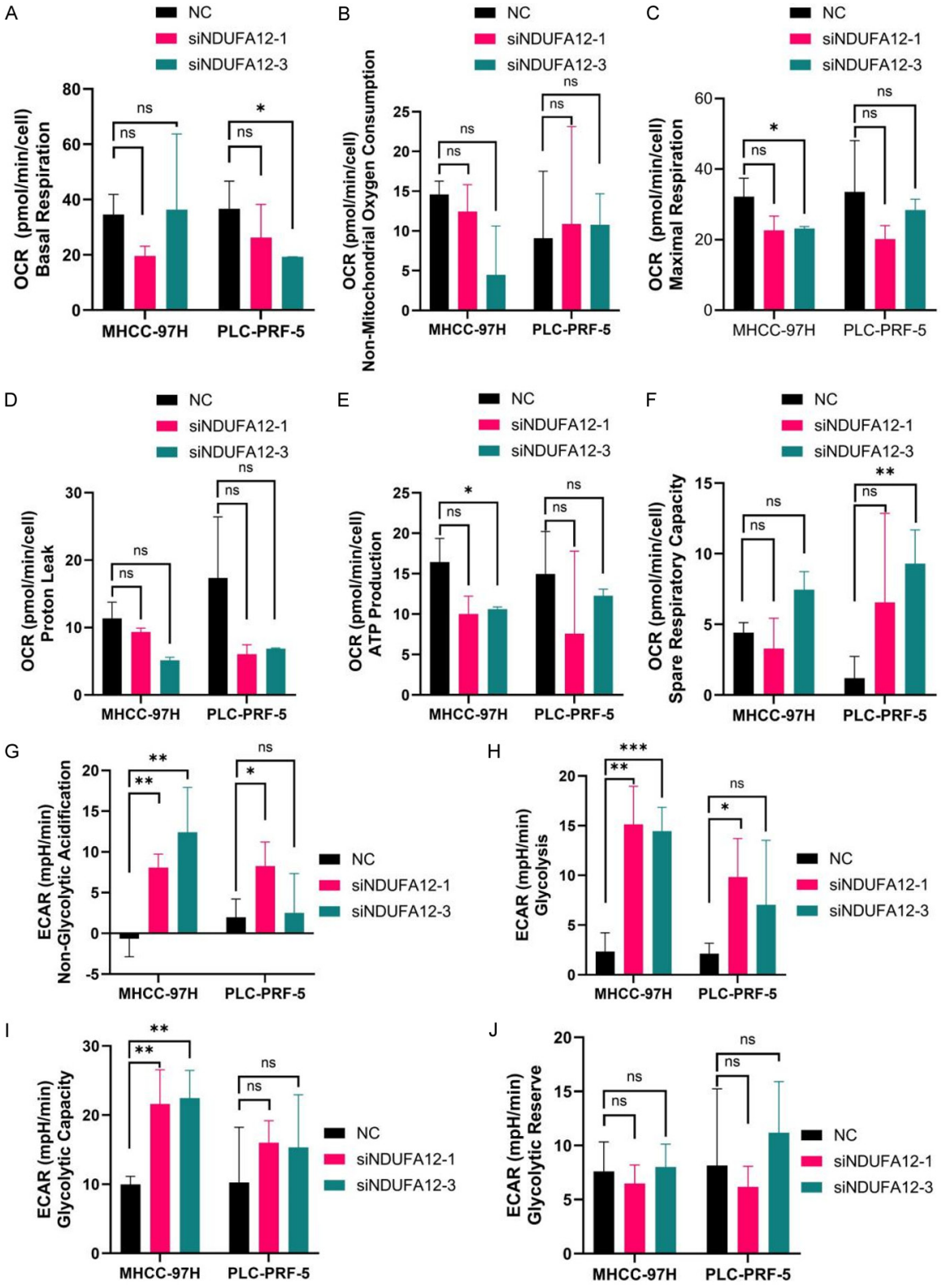

Figure S2. Quantitative analysis of mitochondrial respiration and glycolytic parameters after NDUFA12 knockdown. (A-F) Quantitative analysis of Seahorse XF mitochondrial stress test parameters in MHCC-97H and PLC/PRF/5 cells after NDUFA12 knockdown, including basal respiration (A), non-mitochondrial oxygen consumption (B), maximal respiration (C), proton leak (D), ATP-linked respiration (E), and spare respiratory capacity (F). NDUFA12 knockdown reduced multiple OCR-related mitochondrial respiratory parameters, indicating impaired mitochondrial oxidative

phosphorylation. (G-J) Quantitative analysis of Seahorse XF glycolysis stress test parameters, including non-glycolytic acidification (G), glycolysis (H), glycolytic capacity (I), and glycolytic reserve (J). NDUFA12 knockdown increased glycolysis-related parameters, particularly in MHCC-97H cells, with a similar trend observed in PLC/PRF/5 cells. Data are presented as the mean ± SD. *P < 0.05, **P < 0.01, ***P < 0.001; ns, not significant.

Table S4. The original data of our cohort used in this study

Sample_ID	PFS_ status	PFS_ months	OS_ status	OS_ months	B cell naive_ CIBERSORT	B cell memory_CIBERSORT	T cell follicular helper_CIBERSORT	T cell regulatory (Tregs)_CIBERSORT	NK cell resting_ CIBERSORT	NK cell activated_CIBERSORT	NDUFA12
1	0	9.508197	0	9.508197	0.002268	0	0	0.001583	0.097095	0.000309	3.012279
2	0	12	0	12	0	0	0	0	0	0.002205	4.705912
3	1	13.40984	1	22.95082	0.156238	0	0.134439	0	0.036236	0	3.260623
4	1	6.42623	1	21.21311	0.026832	0	0.015308	0.037638	0.06747	0	4.523995
5	1	3.639344	1	13.40984	0.021827	0	0	0	0	0.10871	4.406918
6	0	13.31148	0	13.31148	0.047995	0	0.044563	0.022777	0.005946	0.073698	5.420866
7	1	3.704918	1	7.081967	0.025426	0.073491	0.045919	0.016349	0	0.1015	5.381363
8	0	21.34426	0	21.34426	0.096695	0	0.021743	0.049463	0	0.08237	4.787647
9	1	5.04918	1	15.27869	0.044858	0	0	0.043077	0	0.101496	4.555693
10	0	12.36066	0	12.36066	0.209679	0	0	0	0.125002	0	3.528321
11	1	27.86885	0	32.09836	0.115232	0	0	0.023366	0.044805	0	4.456195
12	1	30.59016	1	39.60656	0.176635	0	0.026799	0.020808	0	0.063376	5.42196
13	0	22.55738	0	22.55738	0.067904	0	0.029166	0.037086	0	0.039778	5.631637
14	0	23.60656	0	23.60656	0.030056	0	0	0	0	0.104443	4.54422
15	1	8.557377	1	11.14754	0.031811	0.006576	0.000919	0.038818	0	0.040175	5.196965
16	1	6.459016	1	7.540984	0	0.004796	0.013419	0	0	0.113262	5.157969
17	1	23.01639	0	23.01639	0.030541	0	0.043446	0.010549	0	0.027991	5.595047
18	0	31.86885	0	31.86885	0.027357	0	0.042073	0	0.024021	0.056096	4.776851
19	1	0.983607	1	1.081967	0	0.012373	0.01054	0.047495	0	0.081328	4.99222
20	1	13.80328	1	18	0.072294	0	0.127277	0	0	0.067313	5.036877
21	1	14.09836	0	32	0.033265	0	0.004914	0	0.014404	0.000465	3.855372
22	0	5.737705	0	5.737705	0.091844	0	0.048398	0.000883	0	0.058884	4.985218
23	0	10.98361	0	10.98361	0	0	0.008991	0	0	0.056063	4.997274
24	1	2.95082	1	3.934426	0	0	0	0.001832	0	0.052719	5.137831
25	1	3.934426	1	14.36066	0.079905	0	0	0.030699	0.015675	0.019701	4.821924